Harmonic distortion in intracochlear pressure and its analysis to explore the cochlear amplifier[a]

Elizabeth S. Olson[b]
Department of Otolaryngology, Head and Neck Surgery, Columbia University, P & S 11-452, 630 W. 168th Street, New York, New York 10032

(Received 3 September 2003; revised 1 December 2003; accepted 15 December 2003)

Intracochlear pressure was measured close to the basal basilar membrane in gerbil with pure-tone stimulation. This report describes harmonic distortion in the pressure. The harmonic components were tuned in frequency and physiologically vulnerable, implying that they were related to the cell-derived force that sharpens tuning at low levels in healthy cochleae. For stimulus frequencies in the vicinity of the best frequency the harmonic distortion appeared to be produced locally, at the place of measurement. Therefore, it could be explored with a local nonlinear model. The combined model and observations demonstrate two specific points: First, the harmonics in the cell-based force were likely similar in size to the harmonics in pressure (multiplied by area) close to the basilar membrane. This is distinctly different than the situation for the fundamental component, where the cell-based force is apparently much smaller than the pressure (times area). Second, although the fundamental component of the measured pressure was much larger than its harmonic components, the harmonic and fundamental components of the active force were likely much more similar in size. This allows the harmonic components in the pressure to be used as an indirect measure of the active force. © *2004 Acoustical Society of America.* [DOI: 10.1121/1.1645611]

PACS numbers: 43.64.Kc, 43.64.Bt [WPS] Pages: 1230–1241

I. INTRODUCTION

The cochlea is a fluid-filled hose divided along its long axis by a ribbon of sensory tissue and coiled into the shape of a snail. Upon acoustic stimulation, a traveling wave of motion ripples down the ribbon and peaks at a place that depends on the frequency of the stimulus. High frequencies peak in the cochlear base, low frequencies closer to the apex. Observing one position and varying the stimulus frequency, one finds that at frequencies close to the best frequency (b.f.) the phase of the motion shows a rapid accumulation. This phase accumulation is the signature of the slowing of the cochlear traveling wave that accompanies its peaking. An outer hair cell (OHC)-generated force exists in the cochlea that enhances the sensory tissue motion and thus cochlear sensitivity. In the base of the cochlea, with stimulus frequencies close to the b.f., low-stimulus-level motion responses can be enhanced by 40 dB or more relative to high-stimulus-level responses (Robles and Ruggero, 2001). As to be expected, this large degree of compressive nonlinearity is accompanied by harmonic distortion. However, the degree of harmonic distortion in basal displacement is small, at the several percent level for stimulus frequencies close to the b.f. (Cooper, 1998) at a stimulus level of 60 dB SPL. Harmonic distortion has also been measured in the cochlear apex at relatively high stimulus levels (Khanna and Hao, 1999).

This report describes harmonic distortion in the intracochlear pressure in the base of the gerbil cochlea. Close to the sensory tissue's basilar membrane (b.m.) the pressure shared the interesting features of b.m. motion described above: frequency tuning, compressive nonlinearity at frequencies close to the b.f., a phase-vs-frequency response that indicates the presence of the traveling wave, and a low level of harmonic distortion. The harmonics were tuned in frequency, peaking at stimulus frequencies around the b.f. and with sharper tuning at low stimulus levels. The low-stim-level harmonics disappeared into the noise postmortem, just as the low-stim-level enhancement of tuning of the fundamental disappears. High-stim-level harmonics (80 dB SPL and above) changed postmortem, but did not always disappear, although when followed over 2 h they decreased substantially or disappeared. The tuning and physiological vulnerability of the harmonic distortion in pressure link it to the cochlea's nonlinear tuning. The basis for the nonlinear tuning is outer hair cells (e.g., Kiang *et al.*, 1986).

At stimulus frequencies within the best frequency peak the phase-vs-frequency relationship of the harmonics was very similar to that of the fundamental. That means that the harmonics arrived at the place of measurement with the same delay as the fundamental, strongly suggesting that the harmonics were locally generated at the place of measurement. This observation allows the pressure harmonics to be interpreted and analyzed as components of the local cell-derived force (as opposed to having been produced by cellular forces elsewhere in the cochlea and traveling independently to the place of measurement) and used to explore the character of that force.

This exploration is made quantitative with a local nonlinear model of one longitudinal segment of the cochlea. The model is a spring–mass system, with a resistive force that is

---

[a] A preliminary version of this work was presented at the Mechanics of Hearing Meeting in Titisee, Germany in July, 2002, and was published in the meeting proceedings: Olson, E.S. (**2003**). ''Harmonic distortion in intracochlear pressure: Observations and interpretation,'' in: *Biophysics of the Cochlea: From Molecules to Models*, edited by A.W. Gummer (World Scientific, Singapore), pp. 228–236.

[b] Electronic mail: eao2004@columbia.edu

proportional to and opposed to velocity and a nonlinear force that is proportional to a fractional power of velocity. By being proportional to velocity, the nonlinear force adds energy to the system and is an ‘‘active force.’’ The spring is the stiffness of the OCC. The mass is composed of both the fluid mass and the mass of the organ of Corti complex (OCC, the organ of Corti and basilar and tectorial membranes). Because of the fluid mass the pressure close to the OCC is a force within the spring–mass system. In this contribution, the model will be fitted to one set of pressure data in order to draw general conclusions about the size and possible shape of the active force.

This paper has to do with using intracochlear pressure to explore the active cochlear force, and some relevant background on intracochlear pressure and the active force is provided here. The cochlear pressure is composed of two components. The compressive pressure is timed to the in–out compression-rarefaction motion of the stapes and is also known as the ‘‘fast-wave’’ pressure. The pressure that is tied to the motion of the OCC and the adjacent fluid is known as the ‘‘slow-wave’’ pressure (Peterson and Bogart, 1950). The slow and fast waves obtain these designations because the fast wave propagates at the speed of sound in water, about 1500 m/s, whereas the slow wave’s propagation speed is about 9 m/s in the region of the b.f. where the cochlear traveling wave is moving slowly (Rhode, 1971), and was found to be as small as 3.2 m/s in very localized measurements (Ren, 2002). The slow-wave pressure is largest close to the OCC and varies rapidly in space in this region, where the fluid acceleration is greatest (Olson, 1999). It produces a pressure difference across the OCC. In contrast, the fast-wave pressure is nearly equal in space throughout the cochlea and, because it creates no pressure difference across the OCC, it is thought not to cause motion of the OCC.

When making pressure measurements in the fluid the fast wave is of course measured along with the slow wave. Cancellation between the slow and fast waves occurs in the region of the b.f. peak because the slow wave is large in the peak region, goes through rapid phase variations there, and is sometimes out of phase with the fast wave. The cancellation results in pressure notches, discussed in Olson (1998, 2001) and visible in the data below. At frequencies well above the peak the slow-wave pressure is small and the fast-wave pressure dominates it, giving rise to a plateau in pressure phase (see Fig. 3). Even further above the peak there is a plateau in OCC motion as well (e.g., Robles and Ruggero, 2001; Rhode, 1971). This is likely due to nontraveling pressure modes that are present in the vicinity of a cochlear window, natural or unnatural (Steele and Taber, 1979; Cooper and Rhode, 1996). These pressure modes are like the fast wave in that they are timed to the motion of the stapes, but like the slow wave in that they are associated with fluid motion (as opposed to compression).

Moving on to background for the active force: the physiological basis for the active force is outer hair cells (e.g., Robles and Ruggero, 2001; Kiang *et al.*, 1986). How exactly the outer hair cells exert forces that give rise to enhanced tuning is a rich research question. The possibilities for this force have been bounded by several studies. These were used to guide the characteristics for the active force in the model of the current study. The effect of the active force on b.m. motion was largest at low levels (Rhode, 1971) and therefore the active force is assumed to be compressive. The modeling/experimental studies of deBoer and Nuttall (e.g., 2000) indicated that the active force had the character, in terms of impedance, of a negative resistance. This means the active force is in phase with velocity—like a damping force, but instead of resisting the velocity, the active force assists it. Shera (2001) also concluded that the active force had the character of a negative resistance, based on the lack of level dependence in the timing of the zero crossings in the b.m. motion response to a click. Finally, an approximately direct measurement of OCC impedance, and how it changed with stimulus level in a healthy cochlea, showed that the active force was small compared with the passive cochlear forces (Olson, 2001). This was also found in the study of deBoer and Nuttall (2000).

This report grew out of a contribution to the Mechanics of Hearing Meeting in Titisse, Germany in July, 2002 (Olson, 2003).

II. METHODS

A brief description of methods is given here; details have been published (Olson, 1998). The measurements were made in deeply anesthetized gerbils stimulated with tones via a speaker coupled to the ear canal. Stimuli were pure tones, 32 ms in duration. Stimulation levels refer to the sound-pressure level in the ear canal. Intracochlear pressure was measured by inserting specialized pressure sensors through small holes that were hand-drilled in the cochlear bone. Pressure measurements in the scala tympani (s.t.) were made in the first turn of the cochlea where the best frequency (b.f.) was approximately 20 kHz. In s.t. the pressure was measured at a series of distances from the b.m.; this report emphasizes the close measurements within 10 μm of the b.m. The pressure in the scala vestibuli (s.v.) just next to the stapes was measured within seconds of each measurement in the s.t. The pressure responses were averaged ($\sim$100 times) and the averaged responses stored and later analyzed via Fourier transform to find the magnitude and phase at the stimulus frequency (fundamental) and the second and third harmonic frequencies. An antialiasing filter cut off the measured response above 60 kHz; therefore, the third harmonic data are only available up to a 20-kHz stimulus frequency. When referencing phases of the harmonics to those of the fundamental, a small phase adjustment was made to account for the frequency dependence of the phase of the antialiasing filter.

An electrode at the round window measured the compound action potential (CAP) response of the auditory nerve to tone pips, as a monitor of cochlear health.

The pressure sensor consists of a glass capillary with inner and outer diameters 100 and 170 μm, tipped with a gold-coated polymer diaphragm. Light from an LED is delivered via a fiber optic threaded into the capillary, and reflects from the diaphragm. The amount of light returning to the fiber optic for transmission to a photodetector varies linearly with the pressure-induced motion of the diaphragm (Hu *et al.*, 1992). As described previously, the sensors are cali-

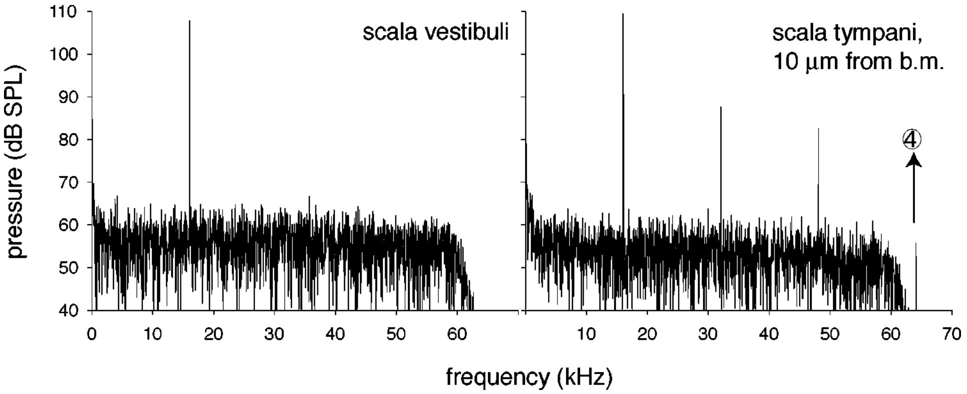

FIG. 1. Pressure spectra, animal 8-28-01. The stimulus was a 16-kHz, 80-dB SPL tone. The s.t. sensor was close to the b.m. (10 μm from it), the s.v. sensor was near the stapes. If the harmonics were associated with the nonlinear mechanics of the organ of Corti, they are expected to be larger in the s.t. pressure close to the basilar membrane than in the s.v. pressure measured near the stapes. This is apparent in the figure, where second, third, and fourth harmonics are visible in the s.t. data but do not emerge from the noise in the s.v. data. The frequency of the fourth harmonic is high enough that it falls above the cutoff frequency of the antialiasing filter. The circled "4" indicates the size of the fourth harmonic after accounting for the attenuation of the filter.

brated by submerging them a known distance beneath the surface of a vial of water which is then shaken with a known acceleration (Bruel & Kjaer model 4290). This produces a known pressure at the position of the sensor. The sensitivity of the sensors is approximately flat (within 3 or 4 dB) up to at least 40 kHz. At a frequency above 40 kHz, the precise value of which varies between sensors, the sensitivity decreases. This is probably due to viscous resistance in the sensor's membrane material. The variation between sensors is likely due to variations in membrane thickness. The drop-off in sensitivity is at high enough frequencies that it does not affect the fundamental response much, but it can affect the harmonics. The sensors are calibrated through 58 kHz, although a resonance in the shaker reduces its reliability above 50 kHz. The primary data set for analysis of this report, the s.t. measurement of Fig. 1, was recorded with a sensor whose cutoff frequency was above 50 kHz, so the sensitivity had decreased very little at the harmonic frequencies and is considered to be flat.

III. OBSERVATIONS

A. Physiological basis for the distortion

The first observations we report tie the distortion to forces within the organ of Corti. When delivering tones into a cavity, the digital-analog/analog-digital (DA/AD) system used in these studies produced harmonic distortion at levels 50 dB below the fundamental. This is not terrifically low (the system has since been upgraded), and several aspects of the data can be used to check that the measured distortion is physiologically based. Because the s.t. pressure was measured close to the OCC, whereas the s.v. pressure was measured near the stapes, if the distortion were generated in the OCC it was expected to be larger in the s.t. measurement than in the s.v. measurement. This is shown in Fig. 1, spectra from animal 8-28-01. This cochlea was mildly nonlinear, with CAP thresholds that were healthy following the initial surgery but elevated by ~15 dB at frequencies around 20 kHz after making the holes to the cochlea. The stimulus was a 16-kHz, 80-dB SPL tone, and the s.t. sensor was close to the b.m. (10 μm from it). Second, third, and fourth harmonics were clearly seen in s.t. but do not emerge out of the noise in s.v.

Changes due to an aging preparation and then postmortem are shown in the spectra of Fig. 2, from animal 4-18-01, a mildly nonlinear cochlea. The measurements were made 10 μm from the basilar membrane with a 17-kHz, 80-dB SPL tone stimulus. A spectrum from data gathered early in the experiment is shown in the left panel (1). The middle panel (2) shows results several hours later, pre-mortem, and the

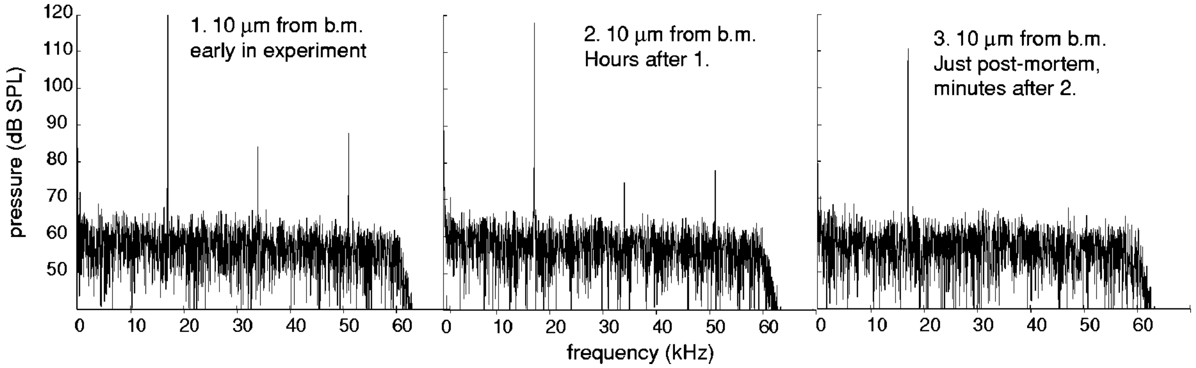

FIG. 2. Pressure spectra, animal 4-18-01. Changes due to an aging preparation and then postmortem. The pressure was measured in scala tympani, 10 μm from the basilar membrane, with a 17-kHz, 80-dB SPL stimulus. A spectrum from data gathered early in the experiment is shown in the left panel. The middle panel shows data gathered several hours later, pre-mortem, and the right panel shows data gathered just minutes later, postmortem.

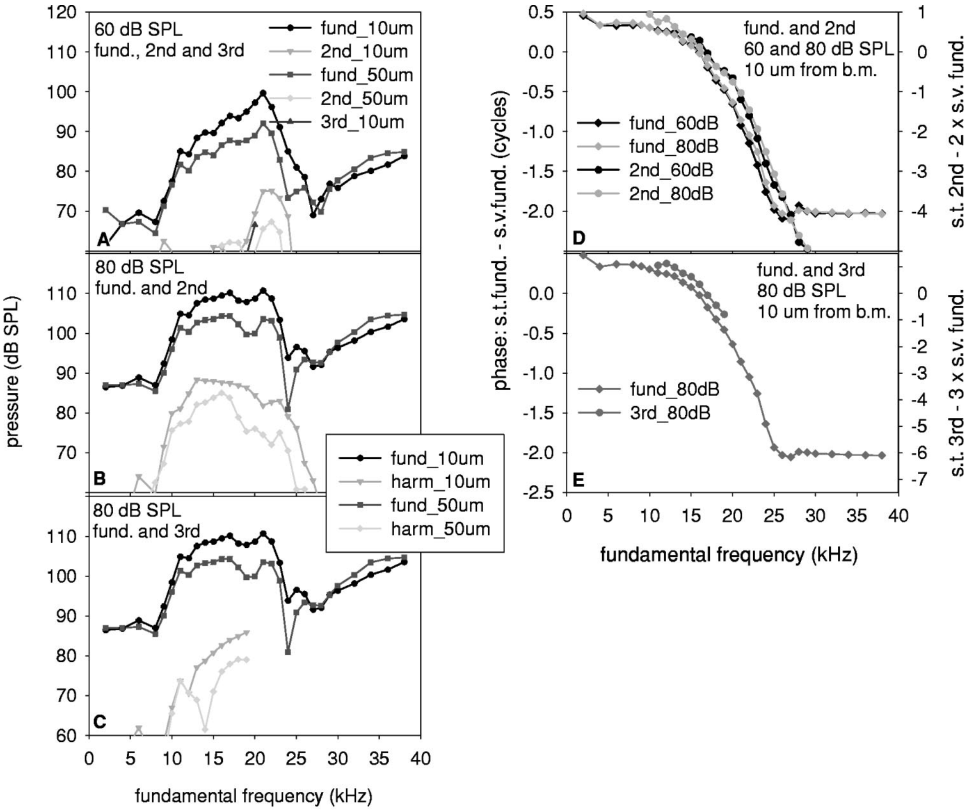

FIG. 3. Scala tympani pressure frequency responses, animal 8-28-01. The magnitude plots [panels (A), (B), and (C)] show the responses at distances 10 and 50 μm from the basilar membrane; the phase plots [panels (D) and (E)] show the response phase at the 10-μm position. Panel (A) shows the fundamental, second, and third harmonic components with 60-dB SPL stimuli. Panel (B) shows the fundamental and second harmonic components with 80-dB SPL stimuli. Panel (C) is similar to panel (B) except the third harmonic is shown. Panel (D) shows the fundamental and second harmonic phases with 60- and 80-dB stimuli. Panel (E) shows the fundamental and third harmonic phases with 80-dB stimuli. The reference for all the phase data was the s.v. pressure fundamental. The s.v. fundamental phase was multiplied by 2 in order to use it for the reference for the s.t. second harmonic, and by 3 in order to use it for the reference for the s.t. third harmonic.

right panel (3) directly (minutes) after the panel (2) data, postmortem. The distortion became smaller with time, and disappeared postmortem.

Another quality of the distortion that speaks for its physiological basis is that the distortion drops off with distance from the b.m. This is seen in Figs. 3 and 5.

B. Frequency sweeps

Frequency sweeps showing the fundamental, second, and third harmonics are shown from three animals. The x axis is the frequency of the fundamental, so the frequencies of the harmonics are 2 and 3 times this frequency.

In Fig. 3 s.t. pressure responses from cochlea 8-28-01, the same cochlea as in Fig. 1, are shown. The magnitude plots (A), (B), and (C) show the pressure at distances 10 and 50 μm from the basilar membrane; the phase plots [(D) and (E)] show the pressure phase at the 10-μm position. In (B) and (C) the sound-pressure level was 80 dB SPL, in (A) it was 60 dB. When the stimulus level was 60 dB the fundamental component showed about 10 dB of compressive nonlinearity compared to the response with the 80-dB stimulus. When the stimulus was reduced to 50 dB SPL there was little additional compression due to the nonoptimal condition of the cochlea. Nevertheless, the compression between 60 and 80 dB SPL produced the characteristic sharpening of the response at the lower stimulus level and thus the OHC force was at work in this preparation. With stimulus levels of 50 (not shown) and 60 dB SPL the second harmonic was a peak positioned in frequency at 20–24 kHz, the frequencies where the fundamental peaked in a broader fashion. When the stimulus level was 80 dB SPL the second harmonic formed a broad plateau between 10 and 25 kHz, with a shape that was similar to the broad tuning of the fundamental. The third harmonic was in the noise when the stimulus level was 50 dB SPL and at 60 dB SPL just emerged from the noise. At 80 dB SPL the third harmonic was broadened in a fashion similar but not identical to that of the second harmonic.

The fundamental and harmonics both decreased with distance from the basilar membrane. The spatial pressure variations reflect fluid motion. ($\nabla p \approx -\rho \mathbf{a}$, where p is pressure, ∇ is the gradient operator, symbolizing spatial differences, ρ is fluid density, and $\mathbf{a}$ is the fluid acceleration. See Olson, 1998, 2001.) One characteristic of note is that the notch that appeared in the fundamental with the 80-dB, 24-kHz stimulus at the 50-μm position did not appear in the harmonic [Fig. 3(B)]. The notch is due to cancellation between the fast-and slow-wave pressures of the fundamental. At the harmonic frequencies, the pressure fell off with distance without a fast-wave–slow-wave cancellation. The observation that the harmonic does not itself notch in the region of the fundamental notch rules out the possibility that the

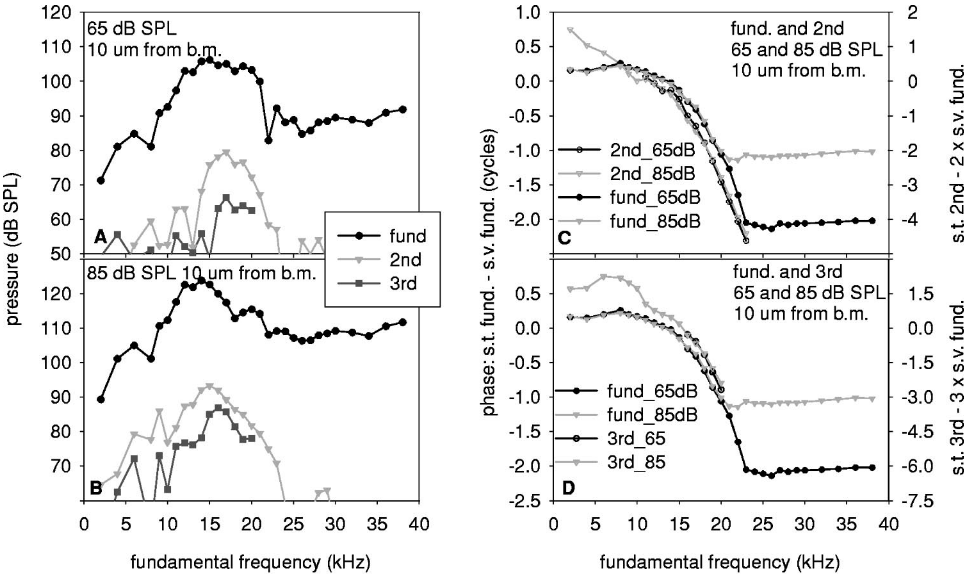

FIG. 4. Scala tympani pressure frequency responses, animal 4-25-00. Responses at 65 and 85 dB SPL, at a position close to the b.m. (10 μm away) are shown. Panel (A) shows the magnitude of the fundamental, second, and third harmonics with 65-dB stimuli, Panel (B) the same with 85 dB stimuli. Panels (C) and (D) show the response phases with 65- and 85-dB stimuli. Panel (C) shows the fundamental and second harmonic, (D) the fundamental and third harmonic.

distortion is an artifact due to nonlinearity in the pressure-sensing membrane.

Figures 3(D)–(E), the phase responses that go along with the 10-μm s.t. pressure magnitudes of Figs. 3(A)–(C), contain one of the principal observations of this study. Figure 3(D) shows the s.t. second harmonic and fundamental phases; Fig. 3(E) shows the s.t. third harmonic and fundamental phases. The phase of each component of the s.t. pressure was referenced to the fundamental component of the s.v. pressure. The s.v. fundamental phase was multiplied by 2 in order to use it for the reference for the s.t. second harmonic, and was multiplied by 3 in order to use it to for the reference for the third harmonic. (That this multiplication of phase is appropriate can be appreciated by thinking of the phase reference as representing an offset in time from the zero phase time of the fundamental s.v. pressure. That time corresponds to a phase that increases linearly with frequency.) The fundamental frequency was plotted on the x axis, so that, for example, the 10-kHz fundamental and its harmonics at 20 and 30 kHz are all plotted at the same x position. The fundamental phase uses the left y axis and the harmonic phase uses the right y axis. The axes of the second and third harmonic phases were expanded by factors of 2 or 3 relative to the y axis of the fundamental phase. The phase plots have the notable characteristic that the phase-vs-frequency slope was nearly the same for the fundamental, the second and the third harmonic. This means that all three components arrived at the point of measurement with the same delay. This strongly suggests that the harmonics were locally generated. In this picture, the fundamental propagates down the cochlea, producing harmonic distortion as it goes. The harmonic distortion does not propagate and therefore the delays of the harmonics measured at a given position are the same as the delay of the fundamental response.

Figure 4 shows frequency sweep data from animal 4-25-00. This was also a mildly nonlinear cochlea. Responses at 65 and 85 dB SPL, at a position close to the b.m. (10 μm away) are shown. The purpose of the figure is to show the repeatability of the results from Fig. 3, namely, tuned harmonics, whose tuning was sharper than the fundamental at the lower stimulus level but became as broad as the fundamental at the higher stimulus level; and harmonic phase-vs-frequency curves that nearly paralleled that of the fundamental. In this cochlea the harmonic phase-vs-frequency slopes deviated from that of the fundamental at low frequencies, 5–10 kHz. The low-frequency deviation might be due to harmonics that were produced basal to the measurement position and traveled to the probe position independently of the fundamental, and with different delays. (However, the third harmonic were nearly in the noise at low frequencies, reducing the reliability of those data.)

The frequency sweeps shown in Fig. 5 were from the healthiest cochlea of this study, (9-8-98), with CAP thresholds that were increased by only about 10 dB following making the holes to the cochlea. In this cochlea at 85 dB SPL [panel (D)] there were two peaks in the second harmonic response, with the upper frequency peak occurring at stimulus frequencies close to the b.f. at the probe position (the usual peak) and a second peak appearing at stimulus frequencies ~ one-half the b.f. The lower peak might be the result of distortion generated basal to the measurement position and traveling to the measurement position, its own b.f. place, where it peaked. This would be the ‘‘amplified distortion’’ reported by Cooper (1998) in measurements of harmonic distortion in b.m. displacement.

The phase data from this cochlea are in Figs. 5(F) and (G). In this cochlea the harmonic phase-vs-frequency curves paralleled that of the fundamental over a relatively restricted frequency range in the region of the b.f. peak. At frequencies below the b.f. peak the lack of similarity means that the distortion was not so closely tied to the fundamental, and might have arrived from other parts of the cochlea. This jibes with the magnitude data described above. The apparent enhanced ability for distortion to propagate in this cochlea might be related to the relative health of the preparation. (Data now emerging from our lab support this view and will be reported in a future publication.) The independently traveling distortion bears further investigation, but not here. In the analysis that follows, the distortion that is generated with stimulus frequencies in the region of the b.f. is explored. As

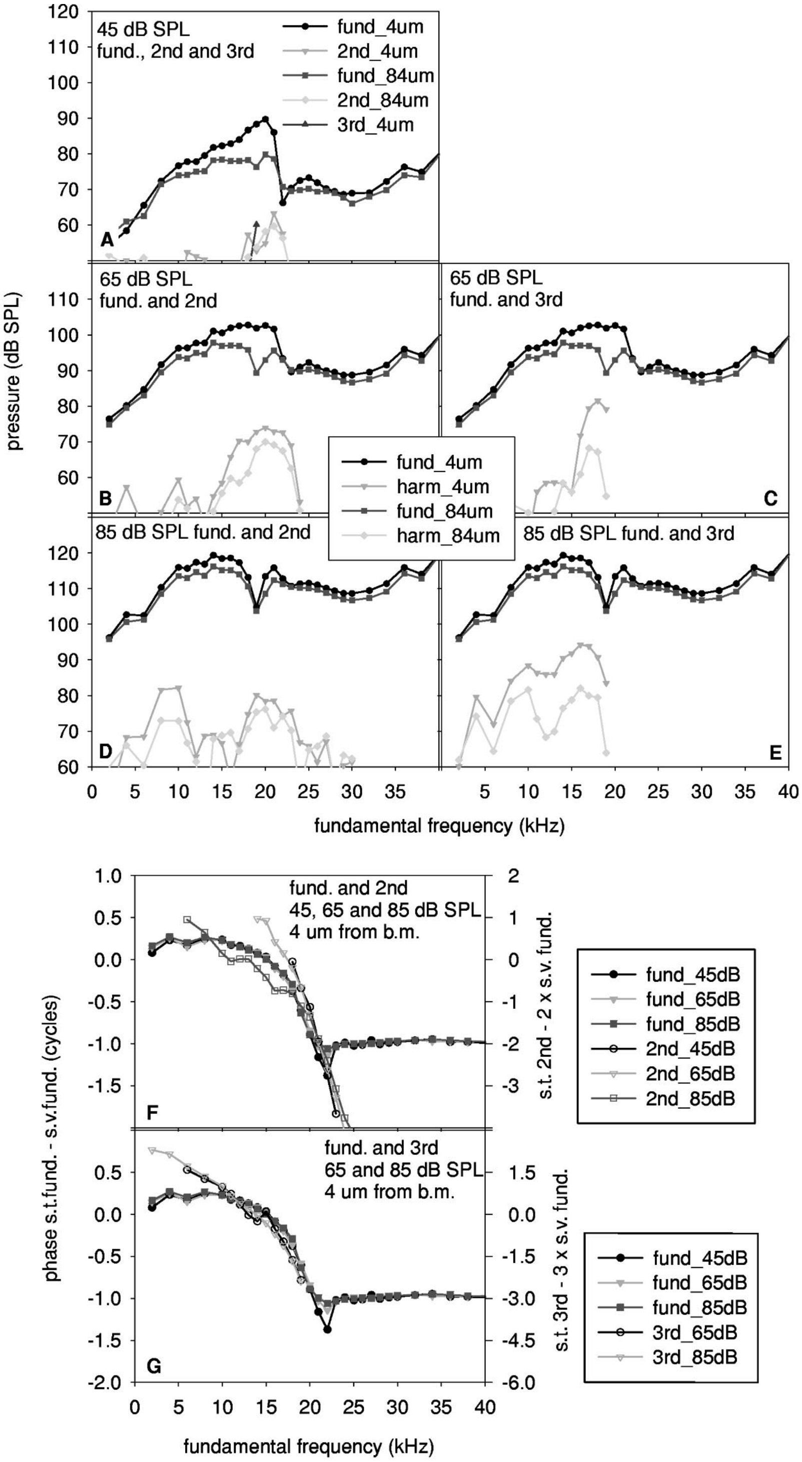

FIG. 5. Scala tympani pressure frequency responses, animal 9-8-98. This was the healthiest animal in this study and had slightly more complicated harmonic behavior seemingly due to an enhanced ability for harmonic distortion, once established, to travel independently of the fundamental traveling wave. The magnitude plots [panels (A)–(E)] show the responses at distances 4 and 84 μm from the basilar membrane; the phase plots [panels (F)–(G)] show the response phases at the 4-μm position. Panel (A) shows the fundamental, second, and third harmonic components with 45-dB SPL stimuli. Panel (B) shows the fundamental and second harmonic components with 65-dB SPL stimuli. Panel (C) is similar to panel (B) except the third harmonic is shown. Panel (D) shows the fundamental and second harmonic components with 85-dB SPL stimuli. Panel (E) is similar to panel (D) except the third harmonic is shown. Panel (F) shows the fundamental and second harmonic phases with 45-, 65-, and 85-dB stimuli. Panel (G) shows the fundamental and third harmonic phases with 65- and 85-dB SPL stimuli.

described above, the phase-vs-frequency behavior of the distortion in this region indicates that it is locally generated—it is a distortion of the fundamental response that has arrived at the place of measurement. This is a requirement of the simple local nonlinear model that is used.

IV. ANALYSIS/MODEL

Consider the cross section sketched in Fig. 6. The forces on the organ of Corti upon acoustic stimulation can be determined by considering this section of the OCC as the mass in the equation expressing Newton's second law, $\Sigma F_{\mathrm{ext}} = m_{\mathrm{oc}} a$. The external forces are exerted on the OCC by the fluid and structures that surround it: The attachment points of the lamina and ligament provide restoring and resistive forces. The fluid pressure of the adjacent fluid, multiplied by the surface area, provides a force that is directed perpendicular to that surface area. The active force is envisioned as arising from the outer hair cells pushing (via the tectorial membrane) between the wall of the inner sulcus, an external structure, and the OCC (Steele and Lim, 1999; deBoer, 1993). We are not concerned with predicting frequency tuning; the response at just one stimulus frequency is examined

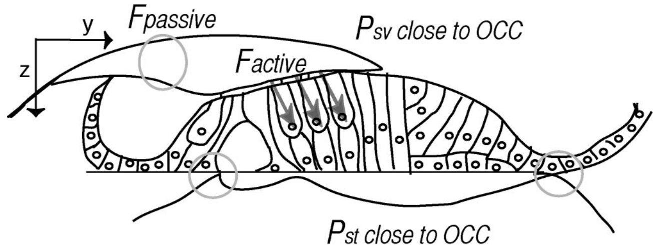

FIG. 6. Cross-sectional sketch of the organ of Corti complex and the forces that govern its motion.

in the model. The strategy is to write force balance for the segment, including a nonlinear active force, and solve the equation in the time domain for the harmonic response in the motion. The distortion in each contributing force is then found and examined. One objective of the model is to demonstrate that although only a small degree of distortion was observed in the pressure close to the b.m., the active force itself probably has a large degree of distortion. The analysis and observations together are used to estimate the size and possible shape of the active force.

The model is based on a 10-μm-long section of OCC, with a width of 200 μm. [Note that 200 μm is approximately the width of the b.m. in turn one of the gerbil cochlea (Plassman *et al.*, 1987) and 10 μm was chosen for the length of a segment, based on the width of hair cells.]
The symbols used in this analysis are as follows:

P_{sv} = scala vestibuli pressure close to the OCC
P_{st} = scala tympani pressure close to the basilar membrane
m_{oc} = mass of the OCC
m_f = effective mass of the cochlear fluid
$m = m_{\mathrm{oc}} + m_f$
$a = \ddot{z}$ = acceleration of the OCC in the z direction
$\dot{z}$ = velocity of the OCC in the z direction
z = displacement of the OCC in the z direction
d = radial width of the OCC
b = longitudinal width of segment of the OCC
$\Lambda = b \cdot d$ = area of segment of the OCC
F_{active} = force exerted by outer hair cells
F_{passive} = passive forces on the OCC
s = stiffness associated with restoring force
R = viscous forces resisting motion of the OCC
$\omega = 2\pi f$, where f is the driving frequency in Hz
F_{drive} = drive force arriving from adjacent basal segment
    $P_{\mathrm{sv\_drive}}$ = associated drive pressure in scala vestibuli
    $P_{\mathrm{st\_drive}}$ = associated drive pressure in scala tympani
    F_0 = amplitude of drive force arriving from adjacent basal segment
λ = wavelength of the cochlear traveling wave
A, v_0, v_w, and ex = parameters that describe the size, range, and offset of the active force.

Force balance in the z direction for the segment is expressed as

$$m_{\mathrm{oc}} a = (P_{\mathrm{sv}} - P_{\mathrm{st}})\Lambda + F_{\mathrm{passive}} + F_{\mathrm{active}}. \tag{1}$$

F_{passive} consists of reactive and resistive components, and the force balance equation is written more specifically as

$$m_{\mathrm{oc}}\ddot{z} = (P_{\mathrm{sv}} - P_{\mathrm{st}})\Lambda - sz - R\dot{z} + F_{\mathrm{active}}. \tag{2}$$

The local pressure difference across the OCC, $P_{\mathrm{sv}} - P_{\mathrm{st}}$, is related to the local fluid motion. In a symmetric cochlear model, $P_{\mathrm{st}} = -P_{\mathrm{sv}}$ and, for an inviscid fluid and small fluid velocities

$$P_{\mathrm{st}}\Lambda = \frac{m_f}{2}\ddot{z}, \tag{3}$$

where m_f is the effective fluid mass per unit length (Steele and Taber, 1979). (The pressure at the OCC both drives the motion of the OCC and the motion of the fluid adjacent to the OCC.) So, the force balance equation becomes

$$m_{\mathrm{oc}}\ddot{z} = -m_f\ddot{z} - sz - R\dot{z} + F_{\mathrm{active}}. \tag{4}$$

Thus, pressure has been replaced by acceleration, which brings the equation closer to a form that can be solved. m_f depends on the local curvature of the traveling wave (curvature $\propto$ 1/wavelength), the width of the OCC, and the size and shape of the cochlear fluid space (Steele, 1987). The curvature of the wave depends on its frequency. For a lightly damped cochlea stimulated at a frequency ω, equating the local kinetic and potential energies of the traveling wave leads to the relationship between the local mass, stiffness, and frequency

$$(m_{\mathrm{oc}} + m_f) = \frac{s}{\omega^2}. \tag{5}$$

(Lighthill, 1983). (While this relationship is for a linear system, for which $|\dot{z}| = \omega|z|$, it is approximately true for the cochlea because of the relatively small size of the distortion. The relationship essentially prescribes the size of the fluid mass so that the traveling wave will exist at the frequency ω.) m_{oc} does not change with frequency; m_f decreases with frequency via changes in the curvature. [Two quick asides about effective fluid mass that are not used here, but are discussed in for example, Lighthill (1981): (i) As an example of effective fluid mass, for a simple 2D wave $m_f \propto \lambda \propto \mathrm{curvature}^{-1}$. Substituting this into Eq. (5) results in a relationship between curvature and frequency that can be used to find the wave's propagation speed. Such a step, followed by an accounting for longitudinal variations in stiffness, is the beginning of a 2D cochlear model. (ii) When the frequency becomes so large that $m_{\mathrm{oc}} \gg m_f$, the wavelength plunges to zero and there is no longer a cochlear traveling wave; in models where m_{oc} is assumed zero, this "cutoff" or "resonant" frequency does not exist.]

The simple analysis of this report models one longitudinal segment and one stimulus frequency. Equation (5) is used to eliminate the mass terms from the force balance equation and get the stimulation frequency into it

$$\ddot{z} = -\omega^2 z - \frac{\omega^2}{s}R\dot{z} + \frac{\omega^2}{s}F_{\mathrm{active}}. \tag{6}$$

Because the model is only of one longitudinal segment, there is no "input." The nonactive model works without an input as long as there is no energy dissipation. Then, the oscillatory motion of the segment goes on and on at frequency ω, just as if a stimulus at that frequency were continuously on, with a size that depends on initial conditions. However, when resistance is present there is energy loss within the segment and, when Eq. (6) is solved with zero active force the result is a damped oscillation. Further insight into how to include an input from the segment basal to our model segment is provided by full cochlear models. Mathematically, when resistance is present in the OCC, the effective fluid mass becomes complex. This can be understood by looking at Eq. (4) in the passive, linear case. The stiffness and mass terms are out of phase and can cancel, but there is not a term to balance the resistive force. Such a term must be present and it arises by m_f becoming complex. Physically, this means that in the damped system the fluid pressure at the OCC is not solely in phase with acceleration, but has a component that is in phase with velocity. This was observed experimentally in Olson (2001). (This component will also arise due to resistance within the fluid (Steele and Taber, 1979), but fluid viscosity is not included here.) In order to include this component of the pressure in our model, a small input force at stimulus frequency ω was added, $F_{\mathrm{drive}}=F_0\cos(\omega t)$. This can be thought of as a fluid pressure arriving from the adjacent basal segment: $F_{\mathrm{drive}}=(P_{\mathrm{sv\_drive}}-P_{\mathrm{st\_drive}})\Lambda=-2P_{\mathrm{st\_drive}}\Lambda$. This last equation will be used after solving the model equation in order to find $P_{\mathrm{st\_drive}}$. $P_{\mathrm{st\_drive}}$ will be added to the P_{st} found from Eq. (3) in order to predict the measured pressure in scala tympani close to the basilar membrane.

We assume a form for the active force of $A[(\dot{z}-v_0)/v_w]^{(ex)}$. The active force is (nonlinearly) proportional to velocity by design, in order that it add energy to the system. This choice was based on cochlear models and experimental analyses (Neely and Kim, 1986; deBoer and Nuttall, 2000; Shera, 2001) in which the mechanism that sharpens the cochlear response at low stimulus levels works by adding energy to the cochlear traveling wave. It is important to note that by making the nonlinear force proportional to velocity, the possibilities for its waveform are restricted—it will be maximum when the velocity is maximum. The free parameters of the model, F_0, A, ex, v_0, and v_w were chosen to provide agreement with the *magnitude* of the spectral components at one stimulus frequency in the region of the b.f. peak, like the data shown in Fig. 1. The phase of the spectral components was not considered. In order to match both the magnitude and phase of the data's spectral components, the form of the active force will need to be relaxed. This is a future study. Finally, the equation that describes the motion of the segment is

$$\ddot{z}=\omega^2\left\{-z-\frac{R}{s}\dot{z}+\frac{A}{s}[(\dot{z}-v_0)/v_w]^{(ex)}+\frac{F_0}{s}\cos(\omega t)\right\}. \tag{7}$$

When this equation is solved, harmonics of the stimulus frequency are generated.

At this point the observation that the phase-vs-frequency curves of the harmonics paralleled that of the fundamental comes into play. The observation means that the harmonics arrived at the place of measurement with the same delay as the fundamental, strongly suggesting that the harmonics were locally generated at the place of measurement. The harmonics were not themselves part of traveling waves at their own frequencies, with their own wavelengths and their own effective fluid masses. Rather, the fluid mass corresponding to the fundamental frequency is envisioned as moving with a distorted time waveform. Then, Eq. (7), whose effective fluid mass corresponds to the fundamental (stimulus) frequency via Eq. (5), applies even though the response contains harmonic frequencies.

To enlarge upon the applicability of the model: It was noted when the data were presented that in the healthiest cochleae (Fig. 5), in addition to the local distortion we can analyze with Eq. (7), propagating distortion components appeared to be present. These components were largest at stimulus frequencies about one-half of the local b.f., where the frequencies of the harmonic components themselves were close to the b.f. In contrast, for stimulus frequencies close to the local b.f. the harmonic frequencies are well above the b.f., and propagating distortion components are not expected to be present. In support of this expectation, at stimulus frequencies close to the local b.f. the phase-vs-frequency data in Fig. 5 are similar to those from Figs. 3 and 4, and indicated that the distortion was local. Therefore, the analysis here is applicable to a healthy cochlea for stimulus frequencies close to the b.f. and is still applicable at frequencies quite a bit smaller than the b.f. when the cochlea is in moderate condition.

The parameter values listed below were based on a 10-μm-long section of OCC, with a width of 200 μm. The analysis models the s.t. pressure data of Fig. 1. Therefore, the stimulus frequency was set at 16 kHz, $\omega=100\,000$ radians/s.

The stiffness was found using the OCC specific acoustic impedance data from Olson (2001). In those results the imaginary part of the impedance had a value that was ~ 10 Pa/(mm/s) at 10 kHz. At this frequency, somewhat below the ~ 20-kHz peak, the imaginary part of the impedance is expected to be primarily determined by stiffness, so we chose to determine its value there. (At frequencies at and above the peak, the imaginary part of the impedance might be reduced from that of stiffness due to proximity to a spring–mass resonance of the OCC stiffness and mass.) To go from this specific acoustic impedance (in units of pressure/velocity) to stiffness (in units of force/displacement) requires multiplying by the area (10×200 μm) and by 2π times 10 000 Hz. The resulting stiffness value is $s=1.2$ N/m$=1.2$ μN/μm. (The last change is made in order to work in units that are more natural for the cochlea.) This value is quite consistent (within about a factor of 2) with the turn one stiffness measured with a blunt, 10-μm-wide stiffness probe (Naidu and Mountain, 1998).

The resistance was found in reference to the impedance data from Olson (2001) and those of deBoer and Nuttall (2000). The high-stim-level impedance data of Olson showed real and imaginary parts of the impedance that were similar in size, although the imaginary part was usually a little bit bigger, sometimes about twice the size of the real part. [See Figs. 15 and 22 of Olson (2001).] If the real part were really

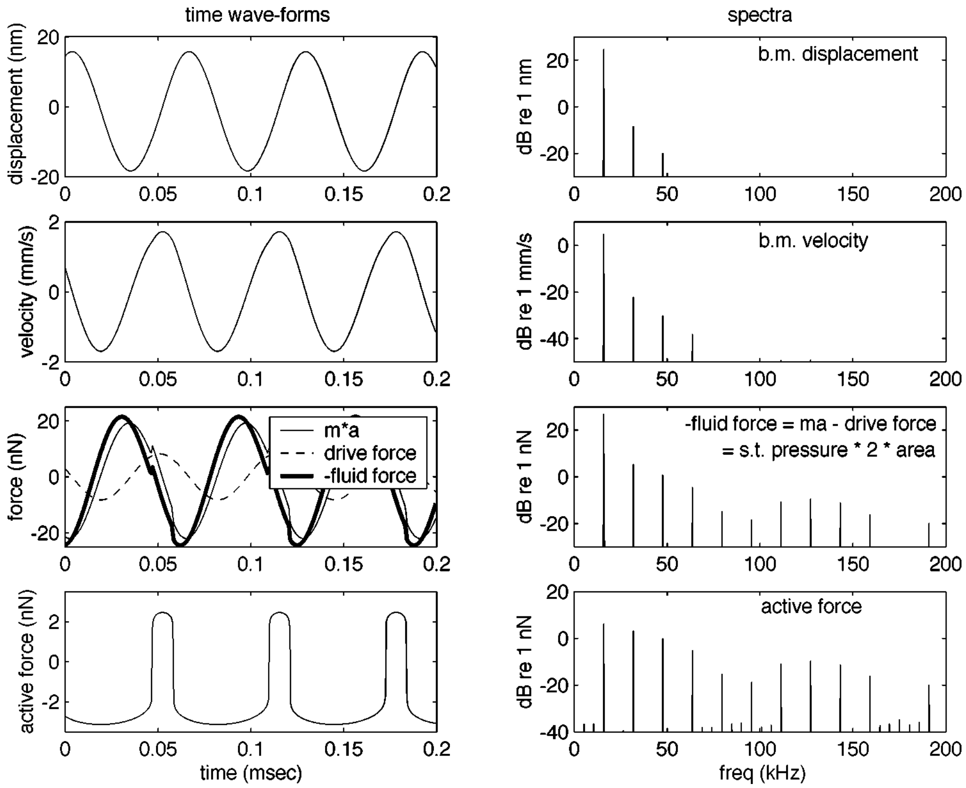

FIG. 7. Model results. The first two rows show the displacement and velocity of the OCC. The left panels show the time waveforms, the right panels show the associated spectra. The dashed line in the third row's left panel shows the drive force. The thin solid line in the third row's left panel shows the acceleration multiplied by m, the mass of both the OCC and fluid. Because the fluid mass is expected to dominate that of the OCC at frequencies below the peak, this is approximately equal to the acceleration multiplied by the fluid mass alone. Following Eq. (3) and the discussion relating the drive force to fluid pressure above Eq. (7), the fluid force on the OCC$=(P_{\mathrm{sv}}-P_{\mathrm{st}})\Lambda=(F_{\mathrm{drive}}-m_f a)\approx(F_{\mathrm{drive}}-ma)$. $ma-F_{\mathrm{drive}}$ is the negative of the fluid force, plotted as the heavy solid line. The negative of the fluid force is plotted in order to begin to relate the modeling results to the experimental observations: $(P_{\mathrm{sv}}-P_{\mathrm{st}})\Lambda=-2\Lambda P_{\mathrm{st}}$, and P_{st} is measured. The fluid force's spectrum is plotted in the right panel. The fourth row shows the active force, time waveform on the left, associated spectrum on the right.

as big as the imaginary part the passive cochlea would be rather heavily damped, which is not the view of most cochlear mechanics theory. The results of deBoer and Nuttall, in the high-stim-level case, showed an imaginary impedance that was about twice the size of the real part. (In both studies, both the real and imaginary parts tended to come down with frequency.) For the purposes of the model here the resistance value was chosen so that the resistive impedance was half the size of the stiffness-based impedance at the stimulus frequency. So, $R\omega=s/2, R=6\cdot 10^{-6}$ μN-s/μm.

The size of F_0 was chosen to give typical response magnitudes in the passive case and to match the data set of Fig. 1. Its value is $F_0=0.0082$ μN.

A, v_0, v_w, and ex determine the size and shape of the active force. Measurements of OCC impedance showed that at moderate levels of stimulus (50–60 dB SPL), even though the active force was causing substantial enhancement in tuning, the fundamental component of the active force was small compared to the restoring force of stiffness (Olson, 2001; deBoer and Nuttall, 2000), and this observation guided the values of the active force parameters. Beyond that, these parameters were chosen in order that the model results matched the observed scala tympani pressure close to the b.m. in Fig. 1—the magnitude of the spectral components. $A=0.0014$ μN, $v_w=1$ μm/s, $v_0=1435$ μm/s, and $ex=\frac{1}{10}$. The individual values of the active force parameters are not likely to be of general significance because their choice was highly dependent on the specific amplitude of the velocity. What is significant and of general interest is the resultant size and obvious distortion of the active force's time waveform.

Equation (7) was solved using MATLAB's ODE45 differential equation solver. (The MATLAB program is available from the author of this paper).

V. MODEL RESULTS

The model results are presented in Figs. 7, 8, and 9. The passive case partner ($A=0$) for Fig. 7 is in Fig. 10.

The four rows of Fig. 7 show displacement, velocity, acceleration recast as fluid force, and active force. The left panels show the time waveforms; the right panels show the associated spectra. The displacement harmonics are at least 30 dB smaller than the fundamental, which compares favorably with Cooper's (1998) result. The velocity harmonics are relatively bigger than the displacement harmonics because velocity scales with displacement times frequency. For the same reason, the acceleration harmonics are relatively bigger than the velocity harmonics. The acceleration in row 3 was recast as force by showing not $\ddot{z}$ but $\ddot{z}(m_{\mathrm{oc}}+m_f)=\ddot{z}\cdot(s/\omega^2)$. If $m_{\mathrm{oc}}\ll m_f$, as it is expected to be except possibly right at and above the peak [some cochlear models argue that m_{oc} is effectively zero (Steele, 1987)], then

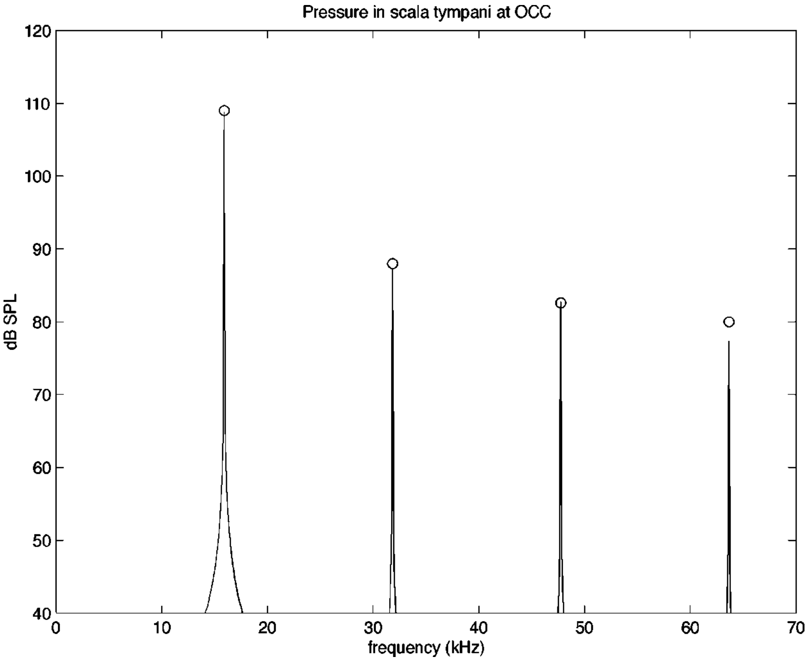

FIG. 8. Model results. The fluid force from the third row of Fig. 7 is divided by 2 times the area of the model segment to find the pressure in scala tympani at the OCC. This can be compared with the experimental measurements of pressure close to the b.m., for example from Fig. 1. The circles show the position of the spectral peaks in the Fig. 1 data, where the fourth harmonic component includes the adjustment for the filter attenuation.

$\ddot{z}\cdot(s/\omega^2)$ is the force that accelerates the effective mass of the fluid. The drive force is also plotted in this panel, as a dashed line. From the discussion leading to Eq. (3) and the discussion on the drive force above Eq. (7), the fluid force on the OCC, $(P_{\mathrm{sv}}-P_{\mathrm{st}})\Lambda$, is composed of two parts. One of the components, $-m_f\ddot{z}\approx-\ddot{z}\cdot(s/\omega^2)$, is in phase with negative acceleration. The second component is the drive force, which was introduced to balance resistive forces. Their sum, $-\ddot{z}\cdot(s/\omega^2)+F_{\mathrm{drive}}=(P_{\mathrm{sv}}-P_{\mathrm{st}})\Lambda=$ the fluid force on the OCC, and the symmetry relationship $(P_{\mathrm{sv}}-P_{\mathrm{st}})\Lambda=-2P_{\mathrm{st}}\Lambda$ relates the fluid force to the measured pressure. The negative of the fluid force is plotted as the bold curve in the same panel. The right-hand panel shows the corresponding spectrum. In Fig. 8 the fluid force is divided by 2Λ, to find the magnitude of P_{st}, the fluid pressure in s.t. close to the OCC, which can be compared with the measured pressure. The circles show the positions of the spectral peaks in the Fig. 1 s.t. pressure data. The agreement is quite good, by design. [As a clarifying note, the fast-wave pressure has not been taken into account in the model because in the frequency region close to the b.f. the slow-wave pressure at the b.m. is bigger than the fast wave pressure (Olson, 2001). Including the fast wave in the model would increase the size of the model's fundamental peak by a few dB, but would not change the harmonics.]

The fourth row of Fig. 7 shows the active force, the time waveform on the left and the associated spectrum on the right. In time it has the shape of a brief impulse that occurs when the velocity is a maximum. The spectral components are large, with the second harmonic just a few dB smaller than the fundamental, and the third and fourth harmonics only decreasing by a few more dB.

Figure 9 shows the dc, fundamental, and second and third harmonic components of all the forces represented in Eq. (7). The time courses of the forces were found using the displacement and velocity solutions shown in Fig. 7. Recall that Fs, the force due to stiffness, $=-s\cdot z$. Fr, the force due to resistance, $=-R\cdot\dot{z}$. FD, the drive force, $=F_0\cos(\omega t)$. FA, the active force, $=A[(\dot{z}-v_0)/v_w]^{(ex)}$. Fm is the mass times acceleration, $\ddot{z}(m_{\mathrm{oc}}+m_f)=\ddot{z}\cdot(s/\omega^2)$. Figure 9 makes clear something that is probably obvious—for each harmonic component of the force–balance equation, force balance must occur. For example, the dc force introduced by the offset in the active force is balanced by a small offset in the position of the OCC, which produces a dc component of Fs.

Looking at the fundamental, Fs is twice the size of Fr; this was by design. Fm balances Fs, and FA and FD both contribute to balancing Fr. Note that FA, the active force, is small compared with Fs, the stiffness force. This is also by design, to be consistent with results of Olson (2001) and deBoer and Nuttall (2000).

Moving on to the harmonics, the phase relationship between Fs, Fm, and Fr is the same as for the fundamental—Fs and Fm are 180° out of phase, Fr is 90° between them. However, Fs and Fm are no longer of equal size. That is because the fluid mass is such that Fm balances Fs at the *fundamental* frequency; therefore, at the second harmonic frequency Fm is four times bigger than Fs. The discrepancy gets bigger as the harmonics gets higher in frequency. The active force must provide force balance for Fm at the harmonic frequencies; i.e., the active force bears most of the responsibility for accelerating the fluid and OCC mass at harmonic frequencies. Therefore, in contrast to the fundamental frequency, where the active force is relatively small, at the harmonic frequencies the active force is relatively large, about the same size as Fm. With the assumption that the fluid mass is much larger than the OCC mass, Fm is approximately equal to the fluid pressure times area. So, the harmonics in the fluid pressure give a good measure of the harmonics in the active force/area. This is clear in the right-hand panels of Fig. 7, in which the harmonics in active force are nearly the same size as the harmonics in the fluid force plotted above it. From the lower panel of Fig. 7, the active

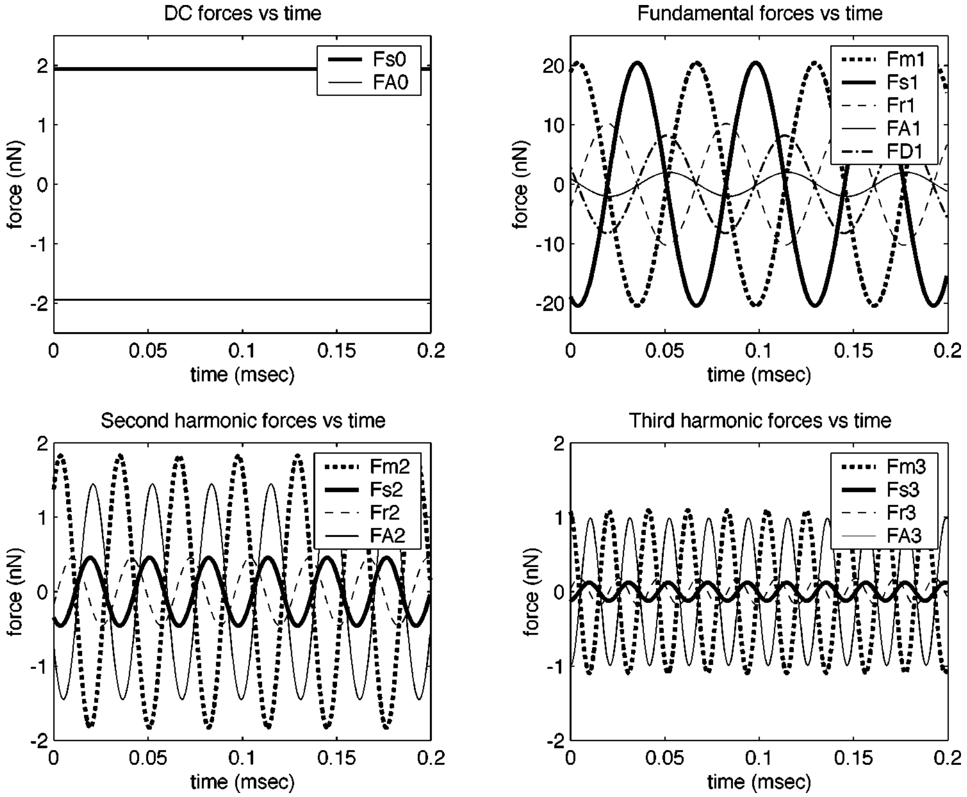

FIG. 9. Model results. The dc, fundamental, and second and third harmonic components of all the forces represented in Eq. (7).

force has a value at the fundamental frequency just over 2 nN, and the second harmonic is just a few dB less; 2 nN corresponds to 660 pN in each of the three outer hair cells in the section. This value can be related to the force that a constrained outer hair cell has delivered *in vitro*: ~100 pN/mV, with a dc whole-cell voltage clamp stimulus (Iwasa and Adachi, 1997), and ~30 pN/mV at frequencies up to at least 50 kHz, with a micro-chamber voltage stimulus (Frank *et al.*, 1999).

Figure 10 shows the displacement, velocity, and fluid forces when the active force is set to zero. Without the nonlinear force no harmonics are generated. The active force did not produce much increase in the fundamental response; a full cochlear model is needed to see its effect (e.g., deBoer and Nuttall, 2000).

The shape of the active force in Fig. 7 brings to mind the image of a child pumping a swing with a swift motion—a brief pulse occurring as the swing (or OCC) passes through its resting position. (Except here it looks more like a parent pushing the swing, as the force occurs at only one point in the cycle, not both coming and going as a swing-pumper would usually do.) Some features of the active force's waveform (e.g., its timing) were produced by model choices that are not settled (e.g., that the active force is proportional to velocity) and might need to be revisited. What is generally illustrated by the model is that to get the series of high-level

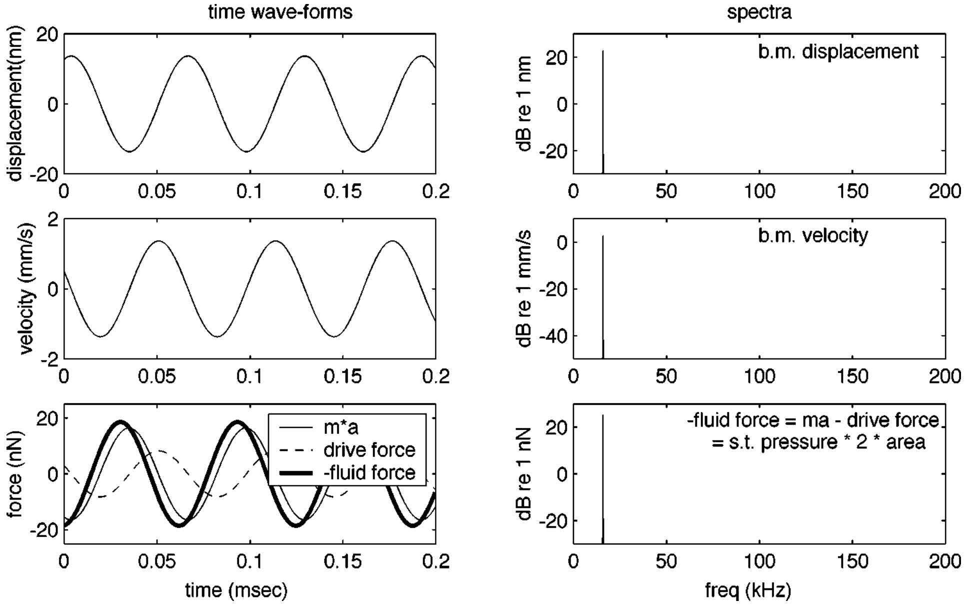

FIG. 10. Model results. This figure is like Fig. 7 except that the active force has been set to zero and therefore no harmonic distortion is produced.

harmonics that is observed (second, third, fourth, ...?), the active force is likely a brief impulse. [A similar point was made by Kemp and Brown (1983) in a study of two-tone emissions.] The impulse-like active force might indicate material decoupling (stereocilia from the tectorial membrane?) cyclically, at high levels of stimulation. Or, it might be intrinsic to the cellular mechanism that produces the active force. In conclusion, the harmonic content of the pressure response close to the b.m. is a measure of the harmonic content of the active force and can be used to predict its size and shape. This knowledge can help guide our understanding of the cellular and structural mechanics of the active force.

ACKNOWLEDGMENTS

This work was supported by NIH DC03130. Thanks to the JASA reviewers and to W. Dong and O. de La Rochefoucauld for helpful comments on the manuscript and to S. Khanna for fruitful discussions.

Cooper, N.P., and Rhode, W.S. (**1996**). ‘‘Fast traveling waves, slow traveling waves and their interactions in experimental studies of apical cochlear mechanics,’’ Aud. Neurosci. **2**, 207–212.

Cooper, N.P. (**1998**). ‘‘Harmonic distortion on the basilar membrane in the basal turn of the guinea pig cochlea,’’ J. Physiol. (London) **509**, 277–288.

deBoer, E. (**1993**). ‘‘The sulcus connection. On a mode of participation of outer hair cells in cochlear mechanics,’’ J. Acoust. Soc. Am. **93**, 2845–2859.

deBoer, E., and Nuttall, A.L. (**2000**). ‘‘The mechanical waveform of the basilar membrane. III. Intensity effects,’’ J. Acoust. Soc. Am. **107**, 1497–1507.

Frank, G., Hemmert, W., and Gummer, A.W. (**1999**). ‘‘Limiting dynamics of high-frequency electromechanical transduction of outer hair cells,’’ Proc. Natl. Acad. Sci. U.S.A. **96**, 4420–4425.

Hu, A., Cuomo, F., and Zuckerwar, A.J. (**1992**). ‘‘Theoretical and experimental study of a fiber optic microphone,’’ J. Acoust. Soc. Am. **91**, 3049–3056.

Iwasa, K.H., and Adachi, M. (**1997**). ‘‘Force generation in the outer hair cell of the cochlea,’’ Biophys. J. **73**, 546–555.

Kemp, D.T., and Brown, A.M. (**1983**). ‘‘An integrated view of cochlear mechanical nonlinearities observable from the ear canal,’’ in *Mechanics of Hearing*, edited by E. deBoer and M.A. Viergever (Martinus Nijhoff, Delft), pp. 75–82.

Khanna, S.M., and Hao, L. (**1999**). ‘‘Nonlinearity in the apical turn of living guinea pig cochlea,’’ Hear. Res. **135**, 89–104.

Kiang, N.Y.S., Liberman, M.C., Sewell, W.F., and Guinan, J.J. (**1986**). ‘‘Single unit clues to cochlear mechanisms,’’ Hear. Res. **22**, 171–182.

Lighthill, J. (**1981**). ‘‘Energy flow in the cochlea,’’ J. Fluid Mech. **106**, 149–213.

Lighthill, J. (**1983**). ‘‘Advantages from describing cochlear mechanics in terms of energy flow,’’ in *Mechanics of Hearing*, edited by E. deBoer and M.A. Viergever (Martinus Nijhoff, Delft), pp. 63–71.

Naidu, R.C., and Mountain, D.C. (**1998**). ‘‘Measurements of the stiffness map challenge a basic tenet of cochlear theories,’’ Hear. Res. **124**, 124–131.

Neely, S.T., and Kim, D.O. (**1986**). ‘‘A model for active elements in cochlear biomechanics,’’ J. Acoust. Soc. Am. **79**, 1472–1480.

Olson, E.S. (**1998**). ‘‘Observing middle and inner ear mechanics with novel intracochlear pressure sensors,’’ J. Acoust. Soc. Am. **103**, 3445–3463.

Olson, E.S. (**1999**). ‘‘Direct measurements of intracochlear pressure waves,’’ Nature (London) **402**, 526–529.

Olson, E.S. (**2001**). ‘‘Intracochlear pressure measurements related to cochlear tuning,’’ J. Acoust. Soc. Am. **110**, 349–367.

Olson, E.S. (**2003**). ‘‘Harmonic distortion in intracochlear pressure: Observations and interpretation,’’ in: *Biophysics of the Cochlea: From Molecules to Models*, edited by A.W. Gummer (World Scientific, Singapore), pp. 228–236.

Peterson, L.C., and Bogart, B.P. (**1950**). ‘‘A dynamical theory of the cochlea,’’ J. Acoust. Soc. Am. **22**, 369–381.

Plassman, W., Peetz, W., and Schmidt, M. (**1987**). ‘‘The cochlea in gerbilline rodents,’’ Brain Behav. Evol. **30**, 82–101.

Ren, T. (**2002**). ‘‘Longitudinal pattern of basilar membrane vibration in the sensitive cochlea,’’ Proc. Natl. Acad. Sci. U.S.A. **99**, 17101–17106.

Rhode, W.S. (**1971**). ‘‘Observations of the vibration of the basilar membrane in squirrel monkeys using the Mossbauer Technique,’’ J. Acoust. Soc. Am. **49**, 1218–1231.

Robles, L., and Ruggero, M.A. (**2001**). ‘‘Mechanics of the mammalian cochlea,’’ Physiol. Rev. **81**, 1305–1352.

Shera, C.A. (**2001**). ‘‘Intensity-invariance of fine time structure in basilar-membrane click responses: Implications for cochlear mechanics,’’ J. Acoust. Soc. Am. **110**, 332–348.

Steele, C.R. (**1987**). ‘‘Cochlear mechanics,’’ in *Handbook of Bioengineering*, edited by R. Skalak and S. Chien (McGraw-Hill, New York), pp. 30.1–30.22.

Steele, C.R., and Taber, L.A. (**1979**). ‘‘Comparison of WKB calculations and experimental results for three-dimensional cochlear models,’’ J. Acoust. Soc. Am. **65**, 1007–1018.

Steele, C.R., and Lim, K.M. (**1999**). ‘‘Cochlear model with 3-dimensional fluid, inner sulcus and feed-forward mechanism,’’ Audiol. Neuro-Otol. **4**, 197–203.